International Journal of Biological Macromolecules 136 (2019) 177–188

Contents lists available at ScienceDirect

International Journal of Biological Macromolecules

journal homepage: http://www.elsevier.com/locate/ijbiomac

Modification of chitosan macromolecule and its mechanism for the removal of Pb(II) ions from aqueous environment

Gutha Yuvaraja [a,b], Yixiong Pang [a,b], Di-Yun Chen [a,b,*], Ling-Jun Kong [a,b,*], Sajid Mehmood [a,b], Munagapati Venkata Subbaiah [c], Devineni Subba Rao [d], Chandra Mouli Pavuluri [d], Jet-Chau Wen [c,e], Guda Mallikarjuna Reddy [f]

[a] Guangdong Provincial Key Laboratory for Radionuclides Pollution Control and Resources, School of Environmental Science and Engineering, Guangzhou University, Guangzhou, 510006, China
[b] School of Civil Engineering, Guangzhou University, Guangzhou 510006, PR China
[c] Research Centre for Soil & Water Resources and Natural Disaster Prevention (SWAN), National Yunlin University of Science & Technology, 123, Section 3, University Road, Douliou, Yunlin 640, Taiwan, ROC
[d] Institute of Surface-Earth System Science, Tianjin University, Tianjin 300072, PR China
[e] Department and Graduate School of Safety and Environment Engineering, National Yunlin University of Science & Technology, 123, Section 3, University Road, Douliou, Yunlin 640, Taiwan, ROC
[f] Ural Federal University, Chemical Engineering Institute, Yekaterinburg 620002, Russian Federation

ARTICLE INFO

Article history:
Received 12 November 2018
Received in revised form 21 March 2019
Accepted 3 June 2019
Available online 04 June 2019

Keywords:
ACSSB@ZnO
Pb(II)
Kinetics
Isotherms
Thermodynamics

ABSTRACT

It is well-known that heavy metals are non-biodegradable and have been showing remarkable impacts on the environment, public health and economics. Because of high toxic tendency, lead (Pb), is one of the foremost considerable hazardous metal with high environmental impacts. Chitosan is a polysaccharide, and can be utilized in wastewater treatment because of its good sorption ability. Amino and hydroxyl groups (C-3 position) on chitosan can serve as electrostatic interaction and complexation sites for metal cations. Chemical crosslinking can effectively enhance the stability of chitosan in acidic media. Hence a novel, cost-effective and eco-friendly ZnO incorporated into aminated chitosan Schiff's base (ACSSB@ZnO) has been synthesized, characterized (BET, XRD, FTIR, SEM, TEM and ^{1}H NMR), and utilized as an adsorbent for the removal of Pb(II) ions from the aqueous environment. The various operating parameters, such as pH (2–8), agitation speed (30–180), adsorbent dose (0.1–0.8 g), contact time (0–140 min), metal ion concentration and temperature (303–323 K) were investigated. The maximum sorption capacity of Pb(II) onto ACSSB@ZnO was found to be 55.55 mg/g. The equilibrium, and kinetic studies suggested that the adsorption process followed the Langmuir isotherm and Pseudo-Second-Order model. Thermodynamic data showed that the sorption process was feasible, spontaneous, and endothermic.

1. Introduction

Contamination of soil, groundwater, sediments, surface water and air with hazardous and toxic chemicals poses substantial effects on human health and the environment [1]. Particularly, the heavy metal, lead (Pb) is placed as one of the three most toxic heavy metals and mostly exists in industrial and agricultural wastewater. Different industrial applications, such as battery, mining, metal plating, pigments, painting, smelting, ammunition, oil refining, photographic materials, and the ceramic glass units are the major sources of lead contamination in waste water [2]. The literature displayed that long term drinking water having a high level of Pb(II) leads to cause of serious disorders such as kidney diseases, nausea, coma, convulsions, cancer, negative effects on metabolism and intelligence [3,4]. Because of these serious hazardous effects of Pb(II) on human health and toxicity in the environment, and as high abundant heavy metal in the geochemical system, it is an urgent prerequisite to remove Pb(II) from the effluents.

Many techniques have been applied for the removal of Pb(II) ions, such as flocculation [5], membrane filtration [6], solvent extraction [7], biosorption [8], chemical precipitation [9], reverse osmosis [10], adsorption [11] etc. But, most of these techniques have some disadvantages like complicated treatment processes, high cost and more energy use. However, adsorption is a much preferable technique among the above stated methods for the removal of heavy metals from polluted waters compared to others, due to ease of operation and cost-effective process [12]. To overcome these limitations, a great amount of effort has been devoted to synthesizing novel, effective, and environmentally friendly adsorbents based on low-cost and natural polymeric materials [13].

Chitosan is one of the vital natural polymer material occurred from polymers families of chitin and can be found in the shells of crustacean like lobsters, crabs, prawns, and shrimps. Chitosan has multi-

* Corresponding authors at: Guangdong Provincial Key Laboratory for Radionuclides Pollution Control and Resources, School of Environmental Science and Engineering, Guangzhou University, Guangzhou 510006, China.
E-mail addresses: cdy@gzhu.edu.cn (D.-Y. Chen), kongl_jun@163.com (L.-J. Kong).

https://doi.org/10.1016/j.ijbiomac.2019.06.016
0141-8130/

applications such as biomedical, biosensor, pharmaceutical, textile, wastewater treatment and biological properties because of their good film forming abilities, biocompatibility, non-toxicity, good water permeability, high mechanical strength, biodegradability, and easy crosslinkage modification due to the presence of reactive hydroxyl and amino functional groups [14]. However, raw chitosan cannot be directly used as an adsorbent because of its solubility in acidic solutions, low thermal resistance, low surface area, and poor mechanical properties [15]. Hence the modifications in the structure of chitosan through reacting with a new entity, results a different derivatives, usually occurred to promote/enhance the adsorption properties.

During the last few decades, nanoparticles had attracted much attention in the field of adsorption as adsorbent materials. Nanoparticles with large specific surface area and high reactivate have been developed as an excellent adsorbents. Nanoparticle mixed chitosan adsorbents have drawn extensive attentions in the field of adsorption and shown extraordinary sorption capacity towards the pollutants because they can exhibit the advantages of combining both nano-materials and chitosan [16]. However, chitosan has weak mechanical and chemical properties where it easily dissolves in dilute acids, and agglomerates to form a gel in aqueous solution. In order to overcome these limitations, the physical and chemical modification needs to be carried out on chitosan.

Chemical cross-linking is an effective method in the absorption phenomena to accomplish new and improved materials with mechanical strength and chemical stability. Generally, the metal sorption capacity of a sorbent decreased with an increase of crosslinking extent due to the loss of some metal binding sites by crosslinking reaction, more difficult diffusion through the cross-linked polymer network and the reduced polymer chain flexibility [17]. Few reports demonstrated the enhancement of sorption capacity of the chitosan had been increased by introducing active functional groups into the chitosan chain through cross-linking method [18]. Furthermore, magnetic chitosan composites are novel materials that exhibit fast adsorption rate, high efficiency, easy to recover and reuse towards various toxic pollutants in aqueous solution. Compared with the traditional adsorbents, magnetic adsorbents possess a uniquely attractive property that permits their rapid and highly effective removal from almost any type of bio-feedstock [19]. A number of adsorbents, including N-maleated chitosan-immobilized TiO_2 nanoparticles [20], PVA/CS beads [21], chitosan crosslinked with epichlorohydrin-triphosphate [22], MR-PVA beads [23], ethylenediamine modified chitosan microspheres [24], xanthate modified magnetic chitosan [25], chitosan modified with cellulose [26], Polyaniline grafted chitosan [27] and chitosan crosslinked with epichlorohydrin [28] have been used for the removal of Pb(II) ions. To the best of the author's knowledge, there is no investigation reported in the literature on the removal of Pb(II) ions by using ACSSB@ZnO.

In the present study, ACSSB@ZnO material was synthesized through chemical crosslinking method, characterized and utilized as an adsorbent material for the removal of Pb(II) ions from aqueous media. The effect of various experimental conditions such as pH, adsorbent dosage, contact time, initial metal ion concentration and temperature were investigated. Isotherm and Kinetic studies were carried out to understand equilibrium data of uptake capacity and kinetic rate of adsorption. The kinetic data follows the pseudo second order reaction and the equilibrium adsorption data were fitted well with the Langmuir isotherm model. The thermodynamic study was done to accomplish more information about the nature, spontaneity and the behavior of the adsorption process.

2. Materials and methods

2.1. Chemicals and reagents

All chemicals used in this study were analytical grade and used without further purification. Chitosan was purchased from Tianjin umbrella science and technology Co., Ltd., China. Terephthalaldehyde, thionyl chloride ($SOCl_2$), thiosemicarbazide, $Pb(NO_3)_2{\cdot}3H_2O$, $Zn(Ac)_2.2H_2O$, HNO_3, HCl, glacial acetic acid, and NaOH were purchased from Tianjin guangfu technology development Co., Ltd., China. Double distilled water was used throughout the experiments.

2.2. Adsorbate preparation

The stock solution was prepared by using the EPA standard method, which involved the addition of HNO_3 to resist the precipitation of Pb(II) ions. Working standard solutions of Pb(II) were prepared by serial dilutions based on the requirement and their pH was adjusted to the required values by adding 0.1 M HCl or 0.1 M NaOH.

2.3. Adsorbent preparation

2.3.1. Preparation of ZnO nanoflakes

At first $Zn(Ac)_2{\cdot}2H_2O$ (10 mmol, 2.195 g) and NaOH (20 mmol, 0.8 g) were dissolved separately in double distilled water. NaOH was added drop by drop at constant stirring (200 rpm) to the $Zn(Ac)_2{\cdot}2H_2O$ solution. The precipitated solid was separated by the filtration and the residue was washed with distilled water and absolutely methanol until the residue free from impurities. Finally, it was dried in a hot air oven for 1 h at 353 k. The ZnO nanoflakes were stored in airtight containers and kept in desiccators for further use.

2.3.2. Preparation of ACSSB@ZnO

The desired amount of chitosan (2 g) was dissolved in acetic acid aqueous solution (2%, v/v) via stirring. Due to the poor solubility of chitosan, the mixture was kept 3–6 h until a clear solution was obtained. A certain amount of terephthalaldehyde (2.81 g) was dissolved in 30 mL of ethanol and it was added drop wise with continuous stirring at room temperature. Then the mixture was stirred at room temperature for 16 h, followed by refluxing for 18 h, which resulted in a pale yellow colored gel. The mass was concentrated under vacuum until almost dryness. Dimethylformamide (DMF, 10 mL) was added to this residue mass and cooled to 0–5 °C. Chitosan modification (Schiff's base formation) may occur through the free amino groups at C_2 position of chitosan with an active aldehyde group of terephthalaldehyde and it was presented in Scheme 1A. The imine bond was formed during Schiff's base formation. This new synthesized material has a particular characteristic, that it does not require the use of an additional crosslinking agent, such as glutaraldehyde whereas the complexing agent (terephthalaldehyde) itself acts as a crosslinking agent. To this Thionyl chloride was added and refluxed for some time. The —OH group at C_3 was turned into the chlorinated chitosan Schiff's base (Scheme 1B). After that thiosemicarbazide was added and the mixture was stirred with a mechanical stirrer at 600 rpm for 7 h at room temperature. Thiosemicarbazide was substituted by replacing chlorine present in chlorinated chitosan Schiff's base to attain the desired aminated chitosan Schiff's base (ACSSB) and it was shown in Scheme 1C. Finally 2 g of ZnO nanoparticles were added to the aminated ACSSB and refluxed properly. After some time the solution was dropped into the 0.1 N NaOH solution. Then the desired product was separated by filtration and triple-washed with methanol and then deionized water to remove excess chemicals and it was named as ACSSB@ZnO (Scheme 1D) for further representation.

2.4. Batch adsorption studies

A series of batch experiments were conducted to explore the effect of pH, adsorbent dose, contact time, initial Pb(II) ion concentration and temperature. This batch adsorption experiments were performed in 100 mL bottles by agitating ACSSB@ZnO with known varied initial concentrations (10–200 mg/L) of Pb(II) solutions in a shaker (200 rpm of agitation speed) at adjusted pH (5.0), contact time (120 min) and temperature (323 K). The pH of each metal ion solution was adjusted to the required values using 0.1 mol/L NaOH or 0.1 mol/L HCl. Adsorption isotherms were also studied by varying the initial Pb(II) concentration from 25 to

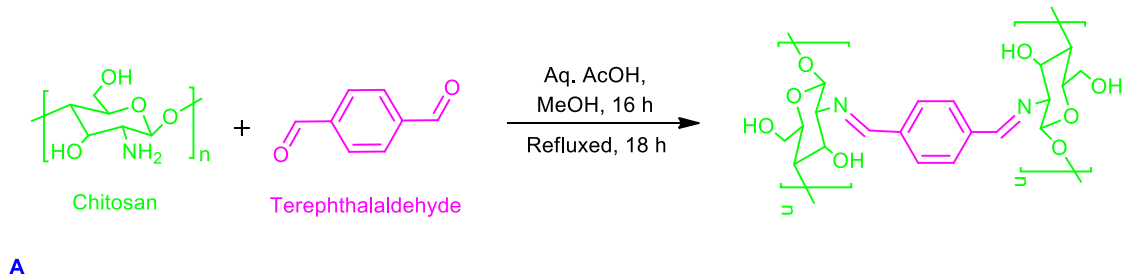

A

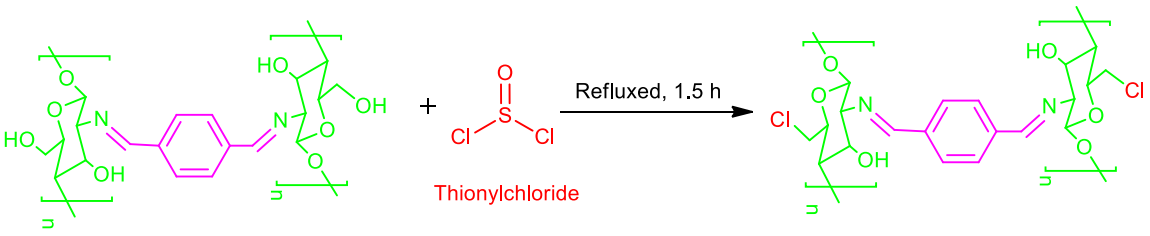

B

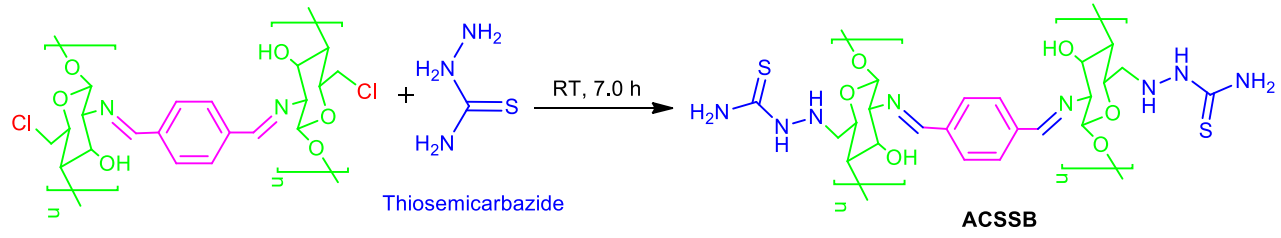

C

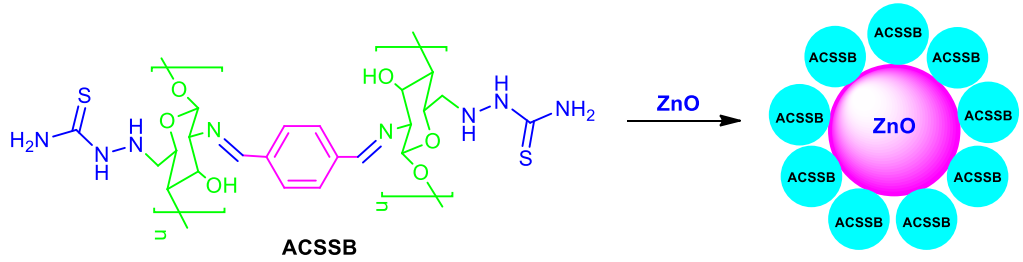

D

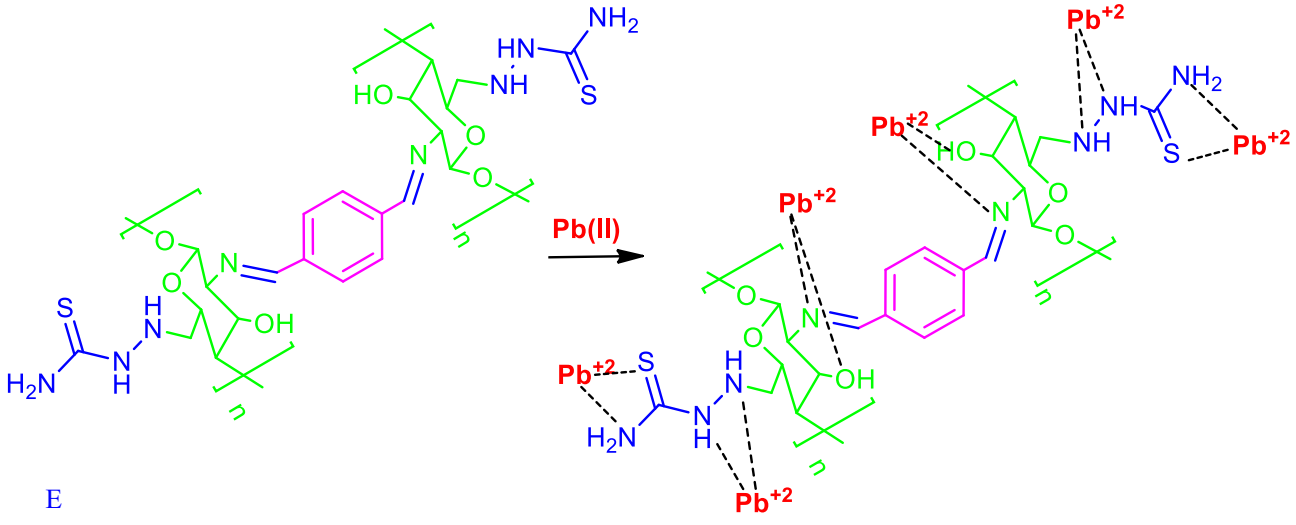

E

Scheme 1. Schematic synthesis of ACSSB@ZnO and its mechanism with Pb(II) ions.

100 mg/L for a fixed amount of adsorbent (0.5 g). The aliquot samples were withdrawn from the shaker and analyzed by using a UV–vis spectrometer. Each experiment was repeated in triplicate and the average values were taken as final results. The amount adsorbed per unit mass of adsorbent at equilibrium was obtained using the equation:

$$q_e = \frac{(C_i - C_e)V}{M} \quad (1)$$

where, q_e (mg/g) is the adsorption capacity at equilibrium, C_i and C_e are initial and equilibrium concentration (mg/L) of Pb(II) respectively, M (g) is the adsorbent dosage, and V (L) is the volume of the solution.

2.5. Metal analysis

The change in Pb(II) ion concentration due to adsorption was determined by UV–vis spectrometer. A brick red color soluble complex was developed by diphenylthiocarbazone in the presence of ammonia in alkaline condition. Absorbance was measured at wavelength 530 nm.

3. Results and discussion

3.1. BET analysis

Surface area, pore volume and pore diameter of ZnO nanoflakes and ACSSB@ZnO were determined by BJH adsorption/desorption method through BET analysis. The BET surface area, pore volume and pore sizes of ZnO nanoflakes were found to be 6.3m^2/g, 0.028cm^3/g and 0.32nm. Whereas ACSSB@ZnO having 11.2 m^2/g, 0.066cm^3/g and 0.62nm of surface area, pore volume and pore sizes.

3.2. XRD analysis

Pure chitosan (Fig. 1A) exhibits two peaks at 2θ = 10 and 20°. Pure ZnO (Fig. 1B) shows the characteristic peaks at (100), (002), (101), (102), (110), (103), (200) and (112) that were in good agreement with wurtzite ore having hexagonal lattice structure [29]. XRD spectra of ACSSB@ZnO (Fig. 1C), exhibits new peaks at 30.1°, 35.5°, 43.1°, 53.5°, 57.0° and 62.6°. This indicates that the ZnO nanoparticles distributed throughout the ACSSB. The main composition of ZnO was not changed during the chemical modification. The aromatic functional groups (terephthaldehyde) were successfully incorporated on the pure chitosan polymer structure. So, it seems that the crystallinity can be regulated by the modification of substituent groups in the chitosan. Hence the XRD results indicate that the ACSSB@ZnO is has a less crystalline structure as compared to pure chitosan.

3.3. FTIR analysis

FT-IR spectrometry is used to characterize the functional groups of the sorbent. Pure chitosan [30] shows (Fig. 2A) the peaks at 3443, 2924, 1652, 1598, 540, 1420 and 1147, 1377 and 1421, 1076 and

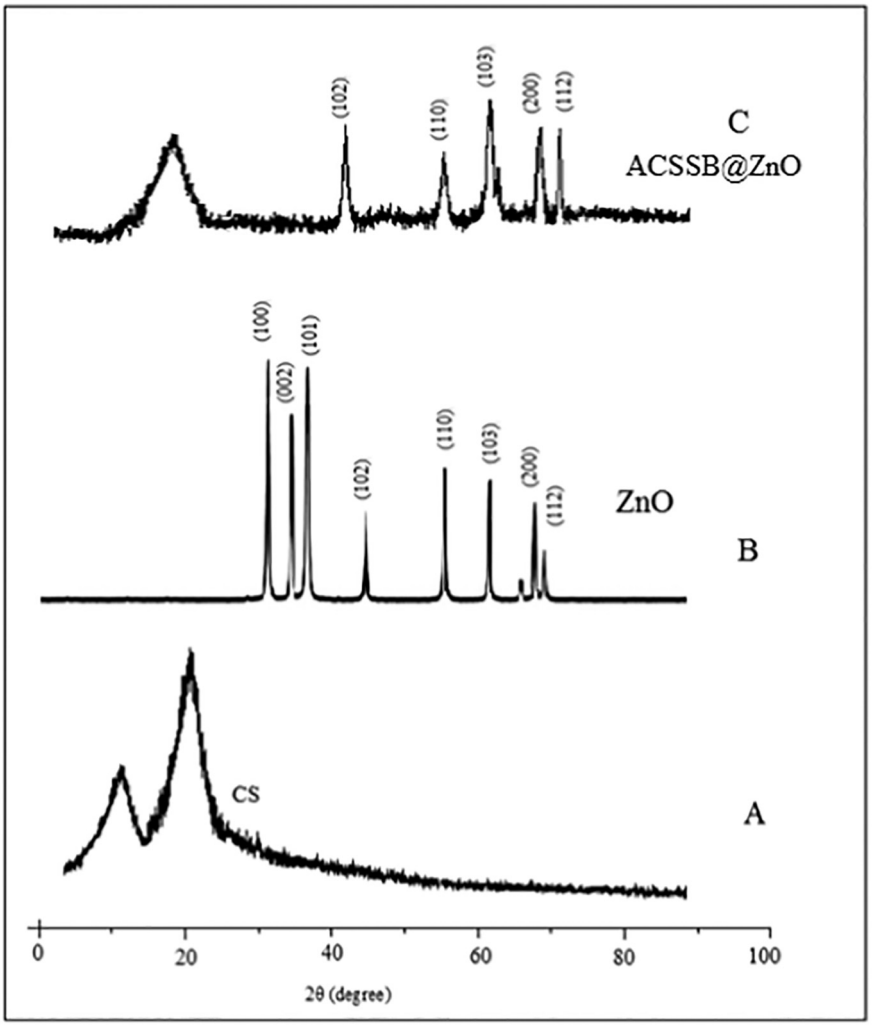

Fig. 1. XRD analysis of (A) pure chitosan, (B) pure ZnO, and (C) ACSSB@ZnO.

1155, 680, 1162 and 987 cm^{-1} represents the stretching vibration of —OH and —NH_2 groups, stretching of —CH group, —C═O, —NH stretching of the secondary amide, N—H angular, C—N axial stretching and N—H angular deformation, methylene and methyl groups, C—O stretching from the β(1 → 4) glycosidic bonds, bending vibration of —OH group are the representative of saccharide ring. The FTIR spectrum of the pure ZnO nanoparticles is shown in Fig. 2B. ZnO nanoparticles exhibits major absorption peaks at 3432, 1596, 1404 and 453 cm^{-1}. Generally metal oxides give absorption bands in the region below 1000 cm^{-1} [31]. The peak at 453 cm^{-1} is attributed to the Zn—O stretching in ZnO lattice [32]. The peaks at 520–750 cm^{-1} assigned to the stretching vibration of Zn—O.

The FTIR spectrum of the pure ACSSB@ZnO shows the peak at 1635 belongs to C═N peak. CH_2-Cl absorption peak at 780 indicates that chlorination was done in chitosan. The peak at 1136 cm^{-1} represents the formation of C-NH bond in ACSSB@ZnO. Whereas the peaks at 520–750 cm^{-1} assigned to the stretching vibration of Zn—O implying that the ZnO nanoflakes were successfully introduced into the ACSSB. After Pb(II) loaded the intensity in the wavenumbers were changed into up and down. The results of FT-IR analysis demonstrated that the adsorption of Pb(II) onto ACSSB@ZnO occurred through chemical interaction, involving hydroxyl, sulphur and amine functional groups may participate in the adsorption process.

3.4. Surface morphological analysis (SEM analysis)

Morphological changes of ACSSB@ZnO before and after adsorption of Pb(II) were studied through SEM analysis. It gives a sufficient general overview of the surface morphology of the adsorbent. The sorption capacity of the adsorbent was mainly due to the difference in their surface structure and surface porosity. Morphological assessment of pure chitosan, ZnO, ACSSB@ZnO and Pb(II) loaded ACSSB@ZnO were depicted in Fig. 3A-D. The surface of the pure chitosan was found to be smooth. Pure ZnO exhibited a nanoflake like morphology. The comparison of SEM images between the ACSSB@ZnO and Pb(II) loaded ACSSB@ZnO showed that Pb(II) had undergone remarkable surface morphology considerably changed after Pb(II) sorption. SEM image of ACSSB@ZnO before metal sorption (Fig. 3C) displayed a smooth plate like structure and it was not observed in Pb(II) loaded ACSSB@ZnO, suggesting that ACSSB@ZnO had undergone remarkable surface morphology considerably changed after Pb(II) sorption.. The rough surface can help increase the surface area available for the removal of Pb(II) ions. This surface morphological changes indicated that metal ion sorption on adsorbent's surface was mediated by the precipitation/complexation of Pb(II) ions with the adsorbent.

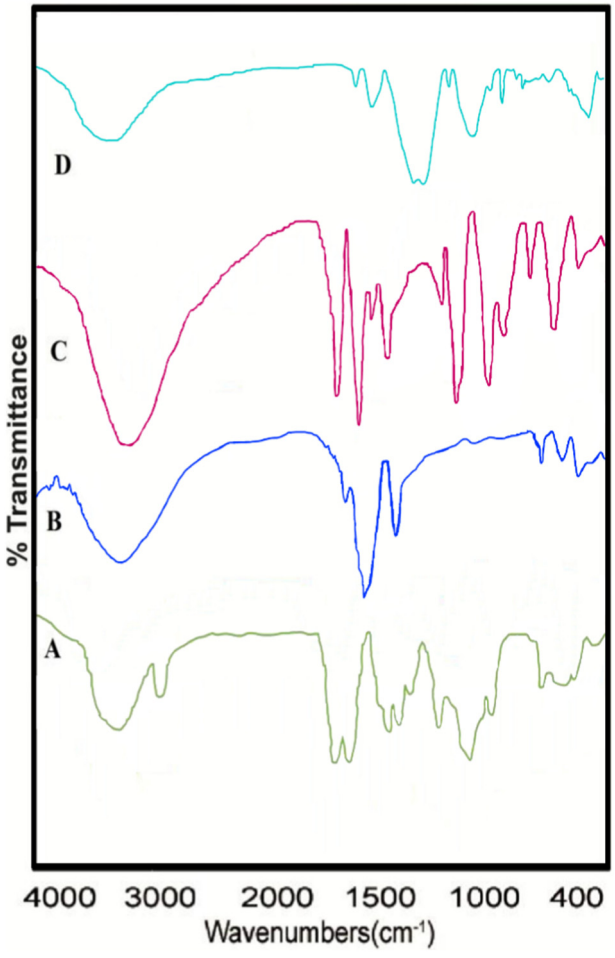

Fig. 2. FTIR spectra of the (A) pure chitosan, (B) pure ZnO, (C) ACSSB@ZnO and (D) Pb(II) loaded ACSSB@ZnO.

3.5. TEM analysis

Transmission electron microscopy (TEM) has been used to identify the size, shape, structure and morphology of nanoparticles. Morphology structure of pure ZnO, ACSSB@ZnO and Pb(II) loaded ACSSB@ZnO were shown in Fig. 4A-C. Fig. 4A and B shows the transmission electron micrographs of pure ZnO, ACSSB@ZnO appeared in flakes like structure (with the scale of 100 and 50 nm). The appearance of the uniformly distributed dark dots (Fig. 4C) with uniform size of particles represents that Pb(II) have been successfully well dispersed in the on the surface of ACSSB.

3.6. ^{1}HNMR analysis

The ^{1}H NMR spectra of the pure chitosan, CSSB, chlorinated CSSB and ACSSB were shown in Fig. 5A-D. Pure chitosan exhibits the well resolved peaks at 4.80 to 1.80. The signals between 3.4 and 4.0 δ correspond to the hydrogen atoms bonded to the carbon atoms 3, 4, 5 and 6 of the glucopyranose unit. The signal centered at 1.99 ppm corresponds to the hydrogen atoms of acetamido methyl groups. Whereas the chitosan Schiff's base (CSSB) ^{1}H NMR spectra (Fig. 5B) exhibits the characteristic peaks of four benzene ring hydrogens at 7.21–7.95 ppm, whereas the peaks at 8.82 ppm belongs to HC═N. The broad signal at 8.82 ppm is assigned to the formation of chitosan Schiff's base (CSSB) between the remained free amino groups of chitosan and aldehyde groups of the cross-linker of terephthaldehyde. In CSSB the aromatic peaks appeared in the range of 7.21–7.95 ppm. Whereas the ^{1}H NMR spectra of 5B exhibited the extra peaks at around 2.3–4.9 ppm belongs to CH_2-Cl group indicated that formation of chlorinated chitosan Schiff's base (CH_2 —OH converted into CH_2-Cl groups) and it was shown in Fig. 5C. Chlorinated chitosan Schiff's base reacts with thiosemicarbazide and forms the final product of ACSSB. The peak at 2.2–4.4 ppm belongs to methylene group indicates that there was no CH_2-Cl bond and it was converted as CH_2-NH bond.

3.7. Effect of pH

pH is one of the most significant variables that affects the speciation of metal ionization/dissociation of the chelating groups and the surface characteristics of modified adsorbents. To investigate the influence of solution pH on the removal efficiency, sorption experiments were carried out at a pH range of 2–8 and the results were shown in Fig. 6A. ACSSB@ZnO contains a large number of amino, sulphur and hydroxyl groups. Most of these groups were protonated easily at low pH value, which was unfavorable to adsorb Pb(II) because of electrostatic attraction or repulsion. At low pH value the electron-donating ability of N, S or O atoms of ACSSB@ZnO was weakened due to the protonation. These leaded to decrease the adsorption capacity of the adsorbent.

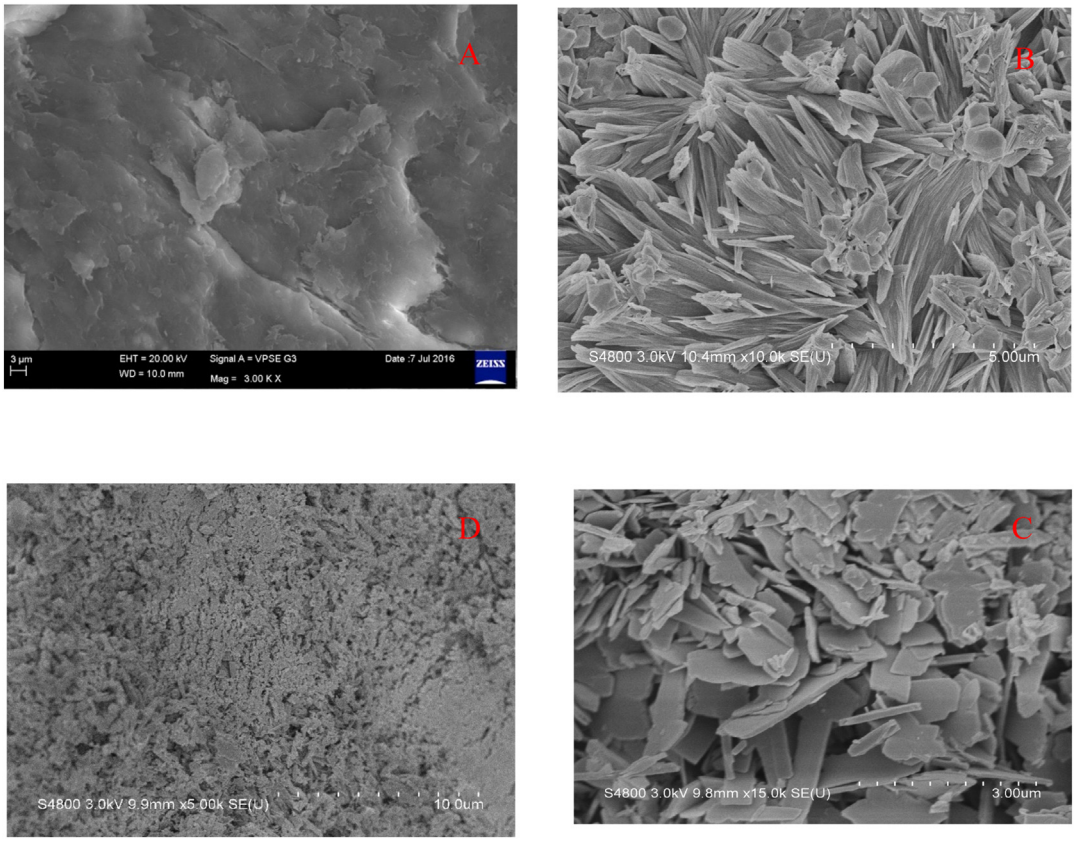

Fig. 3. SEM analysis of (A) pure chitosan, (B) pure ZnO, (C) ACSSB@ZnO and (D) Pb(II) loaded ACSSB@ZnO.

With the increase of pH value, the deprotonation was strengthened. The lower adsorption capacity of Pb(II) ions at low solution pH values were due to the competitive coordination effect of the H ions with N donor atoms of —NH— and O donor atoms of —OH^- on the surface of the adsorbent. The oxygen atom in the hydroxyl group has a stronger attraction to its electron lone pairs over the nitrogen atom in the amino group. Therefore the amino group is more likely to donate the lone pairs to a metal ion [33]. The results revealed that the maximum removal percentage was achieved at a pH of 5.0., and the adsorption studies were not carried out at the pH >5.0 due to precipitation of Pb^2 as Pb $(OH)_2$. Hence, further adsorption experiments were carried out at optimum pH 5.0.

3.8. Effect of agitation speed

Adsorption of Pb(II) ions from aqueous solutions are influenced by agitation speed also. In the present study different agitation speeds (30, 60, 90, 120, 150, and 180) rpm were selected to investigate the effect of agitation speed for the removal of Pb(II) ions onto ACSSB@ZnO. The adsorption rate is also controlled by film and pore diffusion, depending on stirring speed. Low stirring speed results in thicker film layer of the solvent surrounding adsorbent and leads to that this film layer becomes rate controlling step. When the stirring speed is high, the thickness of the solvent film layer gets thinner. Therefore, the movement of the metal ions through the film layer takes place very fast and the diffusion through the pores becomes the rate controlling step [34]. Agitation speed results (Fig. 6B) shows that the sorption capacity reaches to the maximum value at 120 rpm for Pb(II) ions and then decreased afterwards. It can be explained by the fact that the increase in agitation speed, improves internal as well as well as external diffusion of Pb(II) ions towards the surface of the ACSSB@ZnO [35].

3.9. Effect of adsorbent dose

Removal of Pb(II) ions from aqueous solution onto ACSSB@ZnO was studied by varying adsorbent doses from 0.1 to 0.8 g while keeping other parameters such as pH, contact time, temperature and initial metal ion concentration as constant. As shown in Fig. 6C, it was clear that the increase of the dose from 0.1 to 0.6 g, the removal of Pb(II) ions increased from 28% to 96%. The increase in adsorption with adsorbent dosage can be attributed to the higher adsorbent surface and availability of more adsorption sites for the removal of metal ions. This was because that higher adsorbent dose provided more chelating active sites which were exposed in the solution, and the metal ions could have more opportunity to combine with free active groups (oxygen, amine and sulphur). From Fig. 5C it was seen that the maximum removal of Pb(II) ions by ACSSB@ZnO was found to be 0.6 g. After reaching equilibrium there is no considerable change in Pb(II) removal percentage. This may be due to the fact that active sites present in the adsorbent gets completely occupied by the Pb(II) ions and led to the saturation of active sites. Considering the removal efficiency practicality 0.6 g was selected as the optimum adsorbent dose for further studies.

3.10. Effect of contact time

The removal efficiency of Pb(II) ions onto ACSSB@ZnO were also influenced by the contact times. Hence different contact time experiments were conducted in addition to the pH and dose studies. In the present study different contact times (0, 20, 40, 60, 80, 100, 120 and 140 min) were selected to investigate the effect of contact time for the removal of Pb(II) ions onto ACSSB@ZnO and the results were shown in Fig. 6D. The effect of contact time for the removal of Pb (II) ions onto ACSSB@ZnO consisted of three steps, including initial

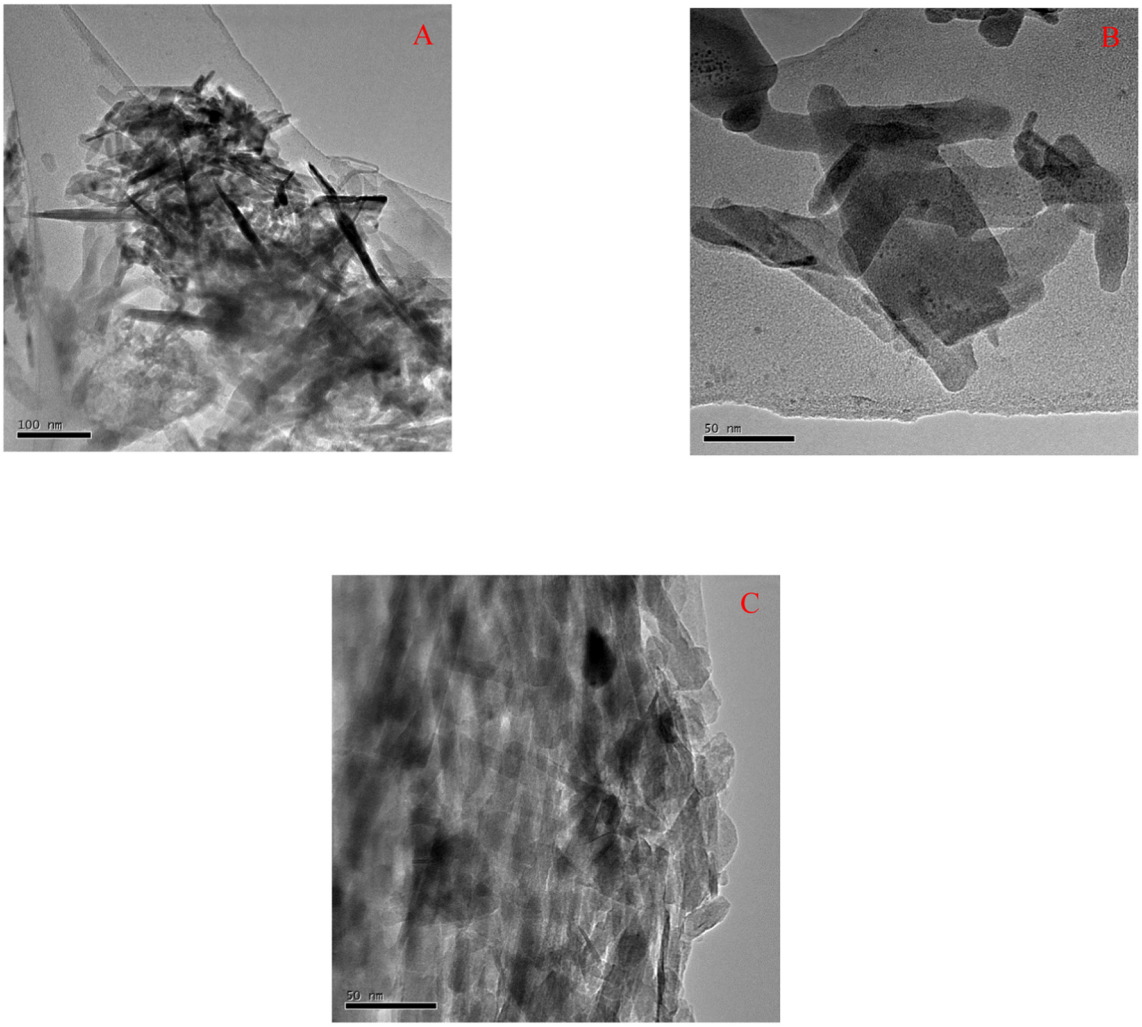

Fig. 4. TEM analysis of (A) pure ZnO, (B) ACSSB@ZnO and (C) Pb(II) loaded ACSSB@ZnO.

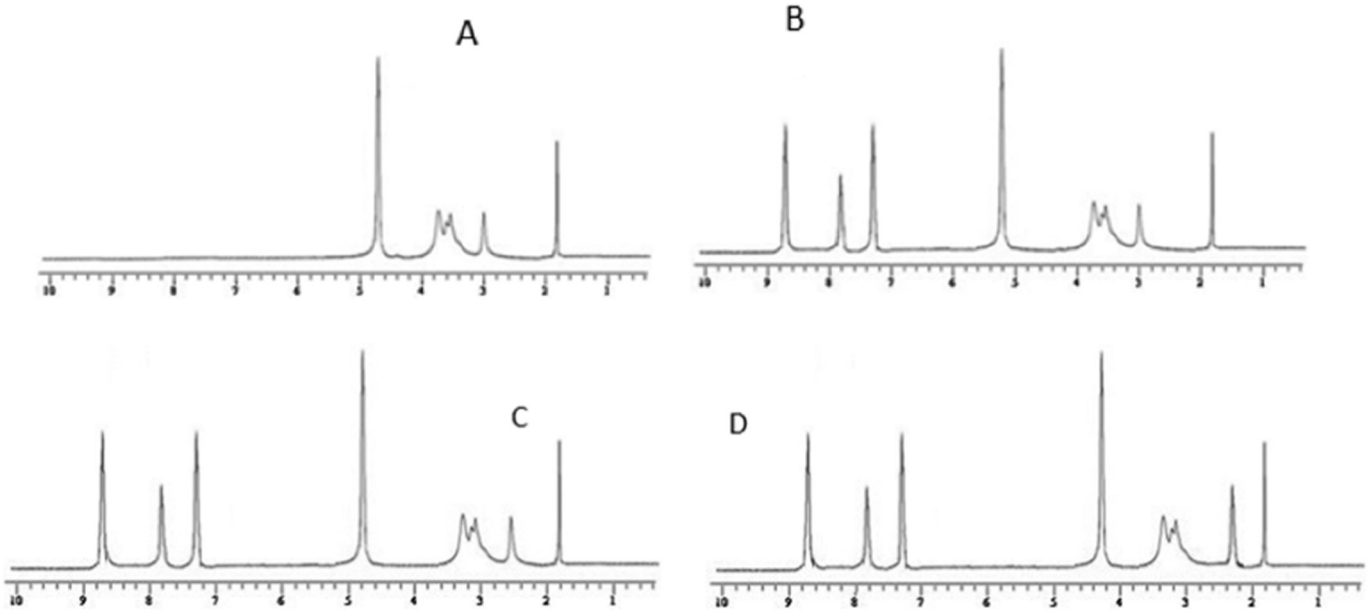

Fig. 5. ^{1}HNMR spectra of (A) pure chitosan, (B) CSSB, (C) chlorinated CSSB and (D) ACSSB.

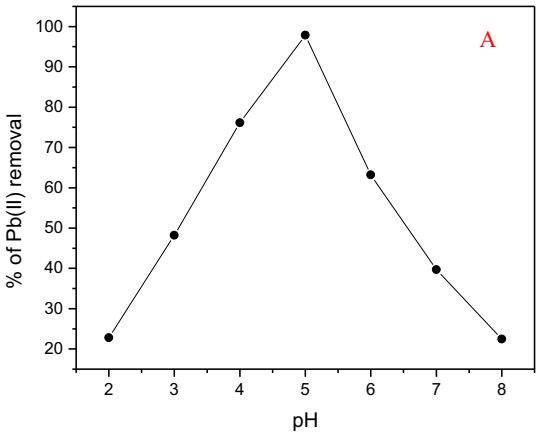
A
% of Pb(II) removal
pH

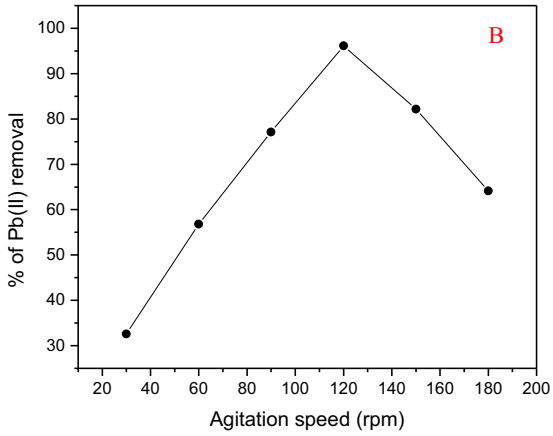
B
% of Pb(II) removal
Agitation speed (rpm)

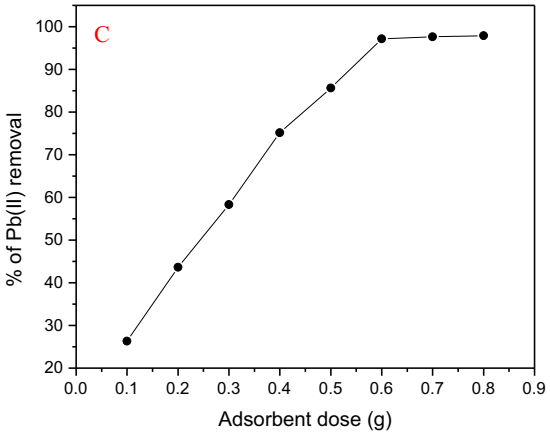
C
% of Pb(II) removal
Adsorbent dose (g)

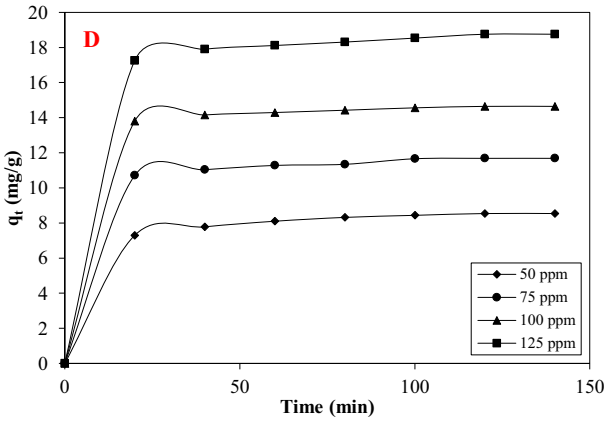
D
q_t (mg/g)
Time (min)
50 ppm
75 ppm
100 ppm
125 ppm

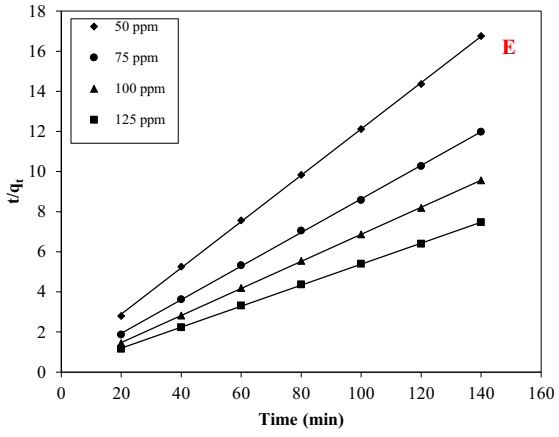
E
t/q_t
Time (min)
50 ppm
75 ppm
100 ppm
125 ppm

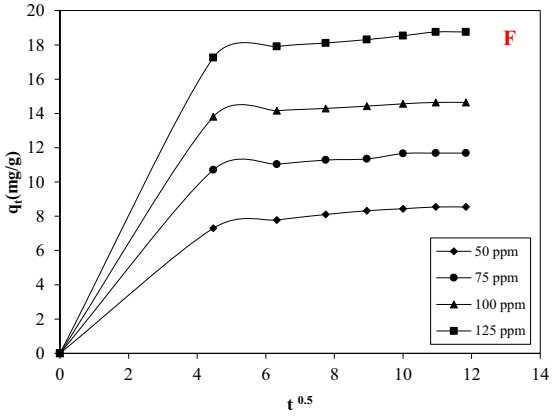
F
q_t(mg/g)
$t^{0.5}$
50 ppm
75 ppm
100 ppm
125 ppm

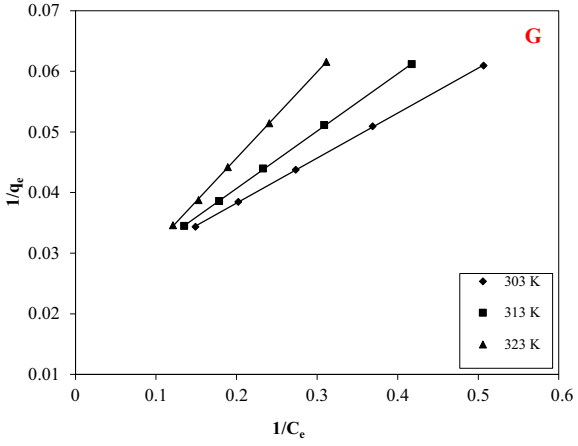
G
$1/q_e$
$1/C_e$
303 K
313 K
323 K

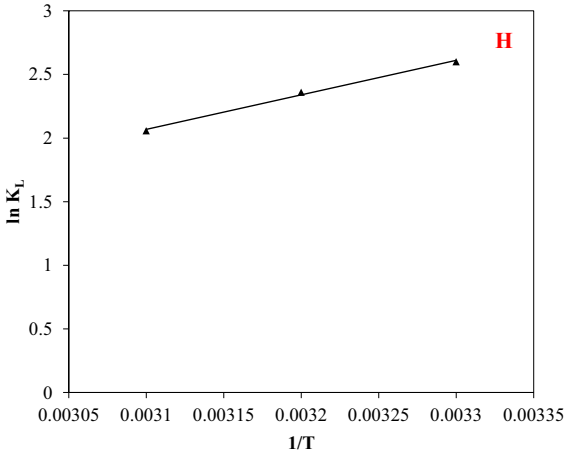
H
ln K_L
1/T

rapid phase which was attributed to the external surface adsorption of metal ions by the adsorbent and second step corresponds to the internal diffusion of metal ions that the metal ions were adsorbed inside the pores of adsorbent. As shown in Fig. 6D, the removal efficiency of ACSSB@ZnO drastically increased in the first 30 min of contact time, especially at high Pb(II) concentrations, and then steadily increased until the adsorption equilibrium was reached. The increase in adsorption capacities during the first 30 min the sorption rate is more and the experiments were continued up to the saturation point obtained (120 min). These results can be due to the fact that at the beginning of the experiment, there were plenty of available active sites on the adsorbent surface, thus facilitating adsorption of Pb(II) ions onto ACSSB@ZnO.

3.11. Effect of initial metal ion concentration

In adsorption phenomena the initial concentration plays a key role as a driving force to overcome the mass transfer resistance between the aqueous and solid phases. The amount of metal ion adsorbed (mg/g) increased with increase in initial concentrations due to higher availability of metal ions for sorption. It can be attributed that the adsorption sites are more in the initial stage, and the Pb(II) ions can interact easily with the active sites of the sorbent. Hence the higher adsorption rate is obtained. The number of active sites in the system is fixed and each active site can adsorb only one ion in a monolayer therefore metal uptake by the sorbent surface is rapid initially and then decreases as the availability of active sites decreases thus slowing down the transfer of a metal ion from the solution to adsorbent surface. The driving force for adsorption is the concentration gradient between the bulk solution and the solid-liquid interface, and the concentration gradient is higher in the initial period, which results in a higher adsorption rate [36].

3.12. Adsorption kinetics study

The prediction of batch adsorption kinetics is one of the significant aspects which can explain the mechanism of adsorption and its potential rate-limiting steps that include mass transport and chemical reaction processes. The adsorption of Pb(II) ions onto ACSSB@ZnO must be considered as a liquid-solid phase reaction which includes diffusion of metal ions from the liquid phase to the surface of the adsorbent, the diffusion of metal ions within the adsorbent and the chemical reaction between metal ions and the functional groups present in the ACSSB@ZnO [37]. To evaluate the kinetic adsorption mechanism different kinetic models were employed to fit the experimental data. In this sense, pseudo-first order [38], pseudo-second order [39], and intra-particle diffusion [40] models were utilized.

The pseudo-first-order model described by the Lagergren and the linear equation is expressed as follows:

$$\log(q_e - q_t) = \log q_e - \frac{k_1}{2.303} t \tag{2}$$

where q_e (mg/g) and q_t (mg/g) are the amounts of Pb(II) sorbed at equilibrium and at time t. K_1 (min^{-1}) is the rate constant of first order sorption process. According to the pseudo-first-order rate equation, the relation between log ($q_e - q_t$) and t should be a straight line and the values of k_1 and qe are calculated from the slope and intercept of that line, respectively. The pseudo-first-order kinetic plot of Pb(II) onto ACSSB@ZnO is not shown and the calculated values of k_1, q_e, and R^2 are presented in Table 1. The low correlation coefficients, R^2, of the pseudo-first-order model for ACSSB@ZnO adsorbent suggest that this model is inapplicable to fit the experimental data.

The kinetic data were further analyzed using Ho's pseudo-second-order kinetic model. The linearized form of the equation is expressed as follows;

$$\frac{t}{q_t} = \frac{1}{k_2 q^2 e} + \frac{1}{q_e} t \tag{3}$$

where q_e and q_t are the amounts of the Pb(II) removal per unit mass of biosorbent (mg/g) at equilibrium and at time t (min), and K_2 (g/mg·min) is the pseudo-second order rate constant. The biosorption rate constant (K_2) is obtained from a linear plot of t/q_t versus t (Fig. 6E) and the values are included in Table 1. The correlation coefficients obtained for the pseudo-second-order kinetic model are >0.999 for all metals. The theoretical q_t values of the pseudo-second-order kinetic model for the sorbent are close to the experimental values than those of the other models. On the other hand, the correlation coefficients for the pseudo-second-order kinetic model are nearly equal to 1 for all initial concentrations of Pb(II) investigated. The pseudo-second-order kinetic model fits the experimental data better than the other kinetic models in this study.

In order to further explore the adsorption mechanism, the experimental data were also fitted to intra-particle diffusion model which was proposed first by Weber and Morris, which is given by eq.4.

$$q_t = K_{id} t^{0.5} + c \tag{4}$$

where q_t (mg/g) is the amount adsorbed at time t (min), K_{id} is the intraparticle diffusion rate constant (mg/g·$min^{-0.5}$) and C is the intercept that gives an idea about the thickness of the boundary layer. The intraparticle diffusion model coefficient values are calculated from the plot of q_t versus $t^{0.5}$ (Fig. 6F) and are given in Table 1. The plot of q_t versus $t^{0.5}$ is a straight line and if it passes through the origin point, thus the intraparticle diffusion is probably only rate-determining step. In the present system, the plot of q_t versus $t^{0.5}$ can be fitted with a straight line but it does not pass through the origin point. Therefore, the intraparticle diffusion is not the only rate-determining step of Pb(II) sorption.

In addition, the sum of square error (SSE) test was carried out to predict the best fit.

$$SSE = \sum \frac{(q_{t,e} - q_{t,m})^2}{q_{t,e}^2} \tag{5}$$

where $q_{t,e}$ and $q_{t,m}$ are the experimental biosorption capacities of metal ions (mg/g) at time t and the corresponding values that are obtained from the kinetic models. SSE values for all kinetic models are calculated and are summarized in Table 1. Pseudo-second-order model has the lowest SSE values when compared with the pseudo-first-order and intraparticle diffusion models. Based on the low SSE values it can be concluded that the sorption of Pb(II) onto ACSSB@ZnO follow the pseudo-second-order model.

3.13. Adsorption isotherms

Adsorption isotherm equations were employed to know the relation and interaction between the amount of solute adsorbed and the concentration of the solute in the fluid phase. Therefore, the correlation of equilibrium data using an equation is essential for practical adsorption operation. The well-known Langmuir [41] and Freundlich isotherm [42] models were applied to study the equilibrium adsorption data. The Langmuir isotherm represents the equilibrium distribution of metal ions between the solid and liquid phases. The Langmuir isotherm

Fig. 6. (A) Effect of pH, (B) effect of agitation speed, (C) effect of adsorbent dose, (D) Effect of contact time at different initial concentrations of Pb(II)ions, (E) Pseudo-Second-Order kinetic plot, (F) Weber-Morris plot at different initial concentrations, (G) Langmuir isotherm plot for the sorption of Pb(II) onto ACSSB@ZnO at different temperatures, and (H) Plot of ln K_L vs. 1/T for the estimation of thermodynamic parameters for the sorption of Pb(II) onto ACSSB@ZnO.

Table 1
Kinetic parameters for the adsorption of Pb(II) onto ACSSB@ZnO at different Pb(II) ion concentrations.

Pb(II) Conc. (mg/L)	Pseudo -first-order			Pseudo-second-order			Weber and Morris		
	K_1 (1/min)	R^2	SSE	K_2 (g/mg·min)	R^2	SSE	K_{id} (mg/g·$min^{-0.5}$)	R^2	SSE
50	0.032	0.989	0.992	0.0228	0.999	0.0016	0.152	0.948	0.9639
75	0.036	0.969	0.993	0.0225	0.999	0.1591	0.233	0.956	0.9605
100	0.036	0.981	0.994	0.0350	0.999	0.0003	0.320	0.986	0.9567
125	0.041	0.962	0.995	0.0189	0.999	0.0006	0.376	0.965	0.9603

(Fig. 6G) model assumes that the uptake of metal ions occurs on a homogenous surface by monolayer adsorption without any interaction between adsorbed ions. The linearized form of the Langmuir isotherm is:

$$\frac{1}{q_e} = \frac{1}{q_m K}\left[\frac{1}{C_e}\right] + \frac{1}{q_m} \tag{6}$$

where q_e is the equilibrium metal ion concentration on the sorbent (mg/g), C_e is the equilibrium metal ion concentration in the solution (mg/L), q_m is the monolayer sorption capacity of the sorbent (mg/g), and K is the Langmuir constant related to the free energy of sorption.

The essential characteristics of Langmuir isotherm model can be expressed in terms of dimensionless constant separation factor R_L, which is used to predict if an adsorption system is 'unfavorable', 'favorable', 'irreversible' or 'linear'. The separation factor R_L can be defined as follows;

$$R_L = \frac{1}{(1 + b\,C_0)} \tag{7}$$

where value of RL indicates that the type of the isotherm either to be unfavorable ($R_L > 1$), linear ($R_L = 1$), favorable ($0 < R_L < 1$), or irreversible ($R_L = 0$).

In Freundlich isotherm model, the adsorption process is not limited to monolayer and the sorption process occurs on a heterogeneous surface by multilayer sorption. The linearized form of the Freundlich isotherm is:

$$\log q_e = \log K_f + \frac{1}{n}\log C_e \tag{8}$$

where K_f (mg/g) is a constant relating the biosorption capacity and $1/n$ is an empirical parameter relating the biosorption intensity. The values of Freundlich constants K_f and 1/n are included in Table 2. The correlation coefficients for the Langmuir isotherm are higher ($R^2 > 0.999$) than the Freundlich isotherm and it demonstrate that the Langmuir isotherm model is more adequate to the proposed adsorption system. It was found that the coefficient values obtained for Freundlich isotherm was found to be lower than Langmuir isotherm model. The result indicates that the equilibrium data was not fitted well with the Freundlich isotherm model. According to the isotherm analysis, the correlation of the experimental data with Langmuir isotherm was more ($R^2 > 0.99$) in comparison with the Freundlich model, thus, it is expected that the adsorption is homogeneous with uniform distribution of adsorption sites and monolayer formation.

Table 2
Langmuir, and Freundlich isotherm constants and correlation coefficients for Pb(II) sorption onto ACSSB@ZnO at different temperatures.

Metal ion	Temp. K	Langmuir isotherm				Freundlich isotherm			
		q_m (mg/g)	K_L (L/mg)	R^2	χ^2	K_f (mg/g)	1/n	R^2	χ^2
Pb(II)	303	43.47	13.47	0.999	4.75	12.16	0.468	0.992	23.60
	313	49.50	10.59	0.999	8.48	10.64	0.510	0.994	31.72
	323	55.55	7.83	0.999	12.78	8.81	0.572	0.994	45.83

3.13.1. Chi-Square analysis

Chi-square test was adopted in order to find the suitability of an isotherm that fits the experimental data. The chi-square statistics is basically the sum of the squares of the difference between the experimental and calculated data from models, with each squared difference is divided by corresponding data obtained by calculation. The equation for evaluating the best fit model is as follows:

$$\chi^2 = \sum \frac{(q_e - q_{e,m})^2}{q_{e,m}} \tag{9}$$

where $q_{e,m}$ is the equilibrium capacity obtained from the model (mg/g) and q_e is the experimental equilibrium capacity (mg/g). As seen in Table 2, lower χ^2 values of Langmuir isotherm model show that the experimental data correlate well with the Langmuir isotherm than the Freundlich isotherm. The best fit to the experimental data from Langmuir isotherm model were deduced from the higher correlation coefficients and lower chi-square values suggesting that the ACSSB@ZnO active sites were homogenously disturbed.

3.14. Effect of temperature

Temperature plays an important role in the biosorption process. Temperature effects were carried out at three different temperatures (303, 313 and 323 K) with an optimum pH value of 5.0 and adsorbent dosage level of 0.6 g. The contact time for adsorption was maintained at 120 min. It can be clearly seen that the amount adsorbed of Pb(II) increased with increase in the temperature (303, 313 and 323) at different initial concentration. The increase in temperature increases the sorption capacity mainly depends on the three factors. At first increasing the temperature increases the diffusion of the metal ions from the bulk solution to the bulk of the biosorbent [43]. Second the increase of temperature increases the increase the ionization of the active functional groups which may increases their activity towards the adsorption of Pb(II) ions from solution [44]. Finally the metal complexation increases at higher temperature.

The basic thermodynamics concept supposes that the reaction is an isolated system, where the system energy cannot be lost or gained and the only driving force is the entropy change. To investigate more information about the mechanism of the adsorption process, the thermodynamic parameters (Gibbs free energy, enthalpy change and entropy changes) for the adsorption of Pb(II) at different temperatures (303, 313 and 323 K) were calculated using Van't Hoff's equations (Eqs. (10) and (11)) and the calculated values were tabulated in Table 3. These parameters were estimated to investigate the

Table 3
Values of thermodynamic parameters for the sorption of Pb(II) onto ACSSB@ZnO.

Metal Ion	Temperature (K)	ΔG^o (kJ/mol)	ΔS^o (J/mol K)	ΔH^o (kJ/mol)
Pb(II)	303	−6.552		
	313	−6.141	0.0527	10.13
	323	−5.526		

spontaneity, feasibility and thermal properties of the adsorption process.

$$\Delta G^{\circ} = -RT \ln K_L \quad (10)$$

$$\ln K_L = -\frac{\Delta H^{\circ}}{RT} + \frac{\Delta S^{\circ}}{R} \quad (11)$$

where, R is the universal gas constant (8.314 J/mol K), T is the temperature (K) and K is obtained by multiplying Langmuir constant K_L and q_m. The changes in enthalpy (ΔH°) and entropy (ΔS°) were estimated from the slope and intercept of the plot of ln K_L versus 1/T (Fig. 6H). The value of ΔG° is the foremost among all, because it defines whether a reaction is spontaneous or not. At all temperatures the ΔG° values are negative. The negative values of ΔG° express the spontaneous nature of ACSSB@ZnO for the removal of Pb(II) ions from the aqueous environment. The positive value of ΔH° indicates that the adsorption process was endothermic. It was also suggesting that the increasing sorption of Pb(II) ions with the increase in temperature. The positive values of ΔS° show the increased randomness at the solid/solution interfaces during Pb(II) adsorption.

3.15. Adsorption mechanism

An effort was attempted to identify the major mechanism of adsorption of Pb(II) onto ACSSB@ZnO. The adsorption capacity of materials is influenced by a number of factors, such as adsorbent dose and size, contact time, agitation speed, temperature, pH, nature of adsorbent, and ionic strength of the aqueous solution. Generally, adsorption capacity increases with increasing the adsorbent dose, contact time, and agitation speed. However, favorable conditions may be different for different materials and adsorptions. Hydroxyl, sulphur and amine functional groups present in ACSSB@ZnO plays an important role in Pb(II) sorption. The involvement of functional groups in the mechanism of Pb(II) sorption system by ACSSB@ZnO was elucidated well with ion exchange, electrostatic attraction, and complexation/coordination. Both the nitrogen and the sulphur groups are having lone pair of electrons that can donate the lone pair of electrons to form the complex with the metal ions through an electron pair sharing. Pb(II) ions break the hydrogen bond of the —OH and —NH_2groups. Then, the O or N provide the lone pair of electrons to the unoccupied orbital of Pb(II) ion to form —O—Pb, —N—Pb, or —CO—Pb binding states. Maybe Complexation/coordination, electrostatic attraction, and precipitation are the main mechanisms involved in Pb(II) sorption by ACSSB@ZnO and it was shown in Scheme 1E.

3.15.1. Complexation/coordination

The metal removal from solution may also take place by complex formation on the surface after the interaction between the metal and the active groups. Sorption of Pb(II) ions by ACSSB@ZnO takes place through both adsorption and formation of coordination bonds between metals and amino and thiocarboxyl groups of the adsorbent. Complexation was found to be the only favorable mechanism responsible for Pb(II) ions through the amino, thiocarboxyl groups found in prepared material.

3.15.2. Precipitation/sedimentation

Coprecipitation on the surface of the sorbent is the mainly mechanism to remove heavy metals in aqueous solution. Among the functional groups, the hydroxyl played a great role in the metal removal by surface coprecipitation.

3.16. Comparison study of ACSSB@ZnO with other adsorbents

The adsorption ability of the proposed adsorbent compared to other applied adsorbents is considered a key feature from a practical point of view. Adsorption capacity, and pH for the removal of Pb(II) ions onto various chitosan based adsorbents [45–51] were compared and summarized in Table 4. As can be observed in the table, the adsorption efficiency of ACSSB@ZnO is higher than that of the majority of the adsorbents reported in the literature. The maximum sorption capacity of the sorbent mainly depends on the nature, structure, functional groups and surface area of the sorbent. The superiority of sorption capacity for the present study was due to the introduction of lot of functional groups in the chitosan back bone structure. Hence we may conclude that, ACSSB@ZnO can be used as an alternative sorbent in place of toxic and more costly adsorbents for the Pb(II) ion removal.

Table 4
Comparison study of ACSSB@ZnO with other sorbents.

Adsorbent	Q_{max}	Reference
Thiol-functionalized magnetic	12.5	45
Chitosan-MAA nanoparticles	11.30	46
Crosslinked chitosan-clay beads	7.93	47
Chitosan(Chitin)/Cellulose Composite	27.31	48
Polyaniline grafted chitosan (PGC)	13.23	49
Chitosan-g-poly(acrylamide)/Cu	38.9	50
CHT/ Montmorillonite	17.18	51
ACSSB@ZnO	55.55	Present study

4. Conclusions

In summary, a novel, low cost, and eco-friendly ACSSB@ZnO were synthesized and utilized as an adsorbent material for the removal of Pb(II) ions from the aqueous environment. ACSSB@ZnO was characterized for its surface area/pore size, phases (crystalline/amorphous), functional groups, morphology studies, and crosslinking conformation reaction by BET, XRD, FTIR, SEM/TEM and ^{1}HNMR analysis. Results of FTIR revealed that the functional groups including —OH or NH_2, and S groups have participated for the sorption of Pb(II) ions from the aqueous environment. Both the nitrogen and the sulphur groups (—O—Pb, and —N—Pb) are having lone pair of electrons that can donate the lone pair of electrons to form the complex with the metal ions through an electron pair sharing. The parameters such as pH (5.0), speed of agitation (120 rpm), adsorbent dose (0.6 g), contact time (120 min), and temperature (323 K) were investigated systematically in batch sorption process. Kinetic studies follows pseudo-second order and the thermodynamic data showed that the sorption process was feasible, spontaneous, and endothermic nature. Equilibrium data fitted well with the Langmuir isotherm, and the maximum sorption capacity of ACSSB@ZnO was found to be 55.55 mg/g at 323 K. This study showed that the ACSSB@ZnO could be a promising adsorbent materials for Pb(II) removal from the aqueous environment.

Acknowledgements

Corresponding author Di-Yun Chen is highly thankful to the National Natural Science Foundation of China (U1501231); The Project of Guangdong Provincial Key Laboratory of Radioactive Contamination Control and Resources (2017B030314182); Science and Technology Program of Guangzhou, China (201804020072) for providing the grant to carry out the research. And Dr. Ling-Jun Kong to Guangdong Province Universities and Colleges Pearl River Scholar Funded Scheme (2018).

References

[1] M.I. Ansari, A. Malik, Bioresour. Technol. 98 (2007) 3149.
[2] G. Yuvaraja, N. Krishnaiah, M.V. Subbaiah, A. Krishnaiah, Colloids Surf. B. 114 (2014) 75.
[3] Y.H. Li, Z. Di, J. Ding, D. Wu, Z. Luan, Y. Zhu, Water Res. 39 (2005) 605.
[4] Z. Guo, L. Dong-di, L. Xian-ke, L. Ya-hui, Q.N. Zhao, L. Meng-meng, Z. Yang-ting, S. Tian- shuai, C. Ma, J. Colloid Interface Sci. 490 (2017) 11.
[5] A.R. Karbassi, S. Nadjafpour, Environ. Pollut. 93 (1996) 257.
[6] L. Fan, C. Luo, Z. Lv, F. Lu, J. Hazard. Mater. 194 (2011) 193.

[7] E. Makrlik, P. Vanura, J. Radioanal. Nucl. Chem. 267 (2005) 233.
[8] A.E. Ofomaja, E.B. Naidoo, S.J. Modise, J. Environ. Manag. 91 (2010) 1674.
[9] M.M. Matlock, B.S. Howerton, D.A. Atwood, Ind. Eng. Chem. Res. 41 (2002) 1579.
[10] M.M. Rao, D.K. Ramana, K. Seshaiah, M.C. Wang, S.W.C. Chien, J. Hazard. Mater. 166 (2009) 1006.
[11] M. Imamoglu, O. Tekir, Desalination 228 (2008) 108.
[12] S. Saxena, S.F.D. Souza, Environ. Int. 32 (2006) 199.
[13] G.Z. Kyzas, P.I. Siafaka, D.A. Lambropoulou, N.K. Lazaridis, D.N. Bikiaris, Langmuir 30 (2014) 120.
[14] A.M. El-Nahrawy, A.I. Ali, A.B.A. Hammad, A.M. Youssef, Int. J. Biol. Macromol. 93 (2016) 267.
[15] Y. Chen, J. Geng, Y. Zhuang, J. Zhao, L. Chu, X. Luo, Y. Zhao, Y. Guo, Carbohydr. Polym. 152 (2016) 327.
[16] Y. Wang, Y. Zhang, C. Hou, M. Liu, J. Taiwan Inst. Chem. Eng. 61 (2016) 292.
[17] A.J. Varma, S.V. Deshpande, J.F. Kennedy, Carbohydr. Polym. 55 (2004) 77.
[18] W.S.W. Ngah, C.S. Endud, R. Mayanar, React. Funct. Polym. 50 (2002) 181.
[19] X. Luo, J. Zeng, S. Liu, L. Zhang, Bioresour. Technol. 194 (2015) 403.
[20] M.A. Shaker, A.A. Yakout, Spectrochim. Acta Part A. 154 (2016) 145.
[21] X. Li, Y. Li, Z. Ye, Chem. Eng. J. 178 (2011) 60.
[22] R. Laus, T.G. Costa, B. Szpoganicz, V.T. Favere, J. Hazard. Mater. 183 (2010) 233.
[23] Y. Zhang, Y. Li, X. Li, L. Yang, X. Bai, Z. Ye, L. Zhou, L. Wang, J. Hazard. Mater. 181 (2010) 898.
[24] P.D. Chethan, B. Vishalakshi, Int. J. Biol. Macromol. 75 (2015) 179.
[25] Y. Zhu, J. Hu, J. Wang, J. Hazard. Mater. 221 (2012) 155.
[26] W.S.W. Ngah, L.C. Teong, M.A.K.M. Hanafiah, Carbohydr. Polym. 83 (2011) 1446.
[27] F. Ferrero, C. Tonetti, M. Periolatto, Carbohydr. Polym. 110 (2014) 367.
[28] A.H. Chen, S.C. Liu, C.Y. Chen, C.Y. Chen, J. Hazard. Mater. 154 (2008) 184.
[29] B. Liu, H.C. Zeng, Nano Res. 2 (2009) 201.
[30] J. Xu, G. Yuvaraja, W. Zhang, Colloids Surf. B. 149 (2017) 184.
[31] H. Kumar, R. Rani, Int. Let. Chem. Phy. Ast. 14 (2013) 26.
[32] S. Zandi, P. Kameli, H. Salamati, H. Ahmadv, M. Hakimi, Physica B 406 (2011) 3215.
[33] L. Jin, R. Bai, Langmuir 18 (2002) 9765.
[34] Y. Nuhoglu, E. Malkoc, Bioresour. Technol. 100 (2009) 2375.
[35] H.N. Bhatti, A.W. Nasir, M.A. Hanif, Desalination 253 (2010) 78.
[36] Y. Jiang, H. Pang, B. Liao, J. Hazard. Mater. 164 (2009) 1.
[37] P. Pal, F.J. Banat, J. Nat. Gas Sci. Eng. 18 (2014) 227.
[38] S. Lagergren, Kungliga Svenska Vetenskapsa-kademiens Handlingar, vol. 24, 1898 1.
[39] Y.S. Ho, G. McKay, Process Biochem. 34 (1999) 451.
[40] W.J. Weber, J.C. Morris, Div. Am. Soc. Civil Eng. 89 (1963) 31.
[41] I. Langmuir, J. Am. Chem. Soc. 40 (1918) 1361.
[42] H.M.F. Freundlich, J. Phy. Chem. A 57 (1906) 385.
[43] F. Gode, E. Pehlivan, Fuel Process. Technol. 86 (2005) 875.
[44] Y. Ren, X. Wei, M. Zhang, J. Hazard. Mater. 158 (2008) 14.
[45] W.T. Gan, L.K. Gao, X.X. Zhan, J. Li, RSC Adv. 6 (2016) 37600.
[46] A. Heidari, H. Younesi, Z. Mehraban, H. Heikkinen, Int. J. Biol. Macromol. 61 (2013) 251.
[47] V.N. Tirtom, A. Dinçer, S. Becerik, T. Aydemir, A. Celik, Des. Water Treat. 39 (2012) 76.
[48] X. Sun, B. Peng, Y. Ji, J. Chen, D. Li, AICHE J. 55 (2009) 2062.
[49] R. Karthik, S. Meenakshi, Chem. Eng. J. 263 (2015) 168.
[50] V.K. Gupta, D. Gupta, S. Agarwal, N.C. Kothiyal, S. Sood, D. Pathania, J. Mol. Liq. 224 (2016) 1319.
[51] W.C. Tsai, B.S. Ibarra, C.C. Kan, C.M. Futalan, M.L.P. Dalida, M.W. Wan, Des. Water Treat. 57 (2016) 9799.